

# Fluorine Abundance Variations in Red Giants of the Globular Cluster M4 and Early-Cluster Chemical Pollution

Verne V. Smith

*National Optical Astronomy Observatory, P.O. Box 26732, Tucson, AZ 85726, USA;  
vsmith@noao.edu*

Katia Cunha

*Observatório Nacional, Rua General José Cristino 77, 20921-400, São Cristóvão, Rio de Janeiro, Brazil; katia@on.br*

Inese I. Ivans<sup>1</sup>

*Department of Astronomy, California Institute of Technology, 1200 E. California Blvd., MS 105-24, Pasadena, CA 91125; iii@astro.caltech.edu*

John C. Lattanzio

*Centre for Stellar & Planetary Astrophysics, School of Mathematical Sciences, PO Box 28M, Monash University, Victoria 3800, Australia; John.Lattanzio@sci.monash.edu.au*

Kenneth H. Hinkle

*National Optical Astronomy Observatory, P.O. Box 26732, Tucson, AZ 85726, USA;  
khinkle@noao.edu*

## ABSTRACT

We present fluorine abundances in seven red-giant members of the globular cluster M4 (NGC 6121). These abundances were derived from the HF (1–0) R9 line at  $2.3357\mu\text{m}$  in high-resolution infrared spectra obtained with the Phoenix spectrograph on Gemini-South. Many abundances in the target stars have been studied previously, so that their overall abundance distributions are well-mapped. The abundance of fluorine is found to vary by more than a factor of 6, with the  $^{19}\text{F}$  variations being correlated with the already established oxygen variations, and anti-correlated with the sodium and aluminium variations. In this paper

---

<sup>1</sup> Hubble Fellow

we thus add fluorine to the list of elements known to vary in globular cluster stars, and this provides further evidence that H-burning is the root cause of the chemical inhomogeneities. The fact that  $^{19}\text{F}$  is found to decrease in the M4 stars, as the signature of H-burning appears, indicates that the polluting stars must have masses greater than about  $3.5M_{\odot}$ , as less massive stars than this should produce, not destroy, fluorine.

*Subject headings:* nucleosynthesis–stars: abundances

## 1. Introduction

Many galactic globular clusters display abundance patterns not observed among field stars possessing similar masses and metallicities. In a given cluster, star to star abundance variations may be observed among a specific, small set of light elements: C, N, O, Na, Al and sometimes Mg. Within a given cluster, the C and N abundances are anti-correlated, while O and Na, as well as Al and Mg, are also anti-correlated. Such anti-correlations can be understood to result from H-burning (or proton captures) among the various reaction networks known as the CNO cycles, the Ne-Na cycle, and the Mg-Al cycle. With each progressive set of cycles among increasingly charged nuclei, the H-burning samples ever hotter regions within a star. An extensive review of these abundance patterns, along with their corresponding large set of literature, can be found in Gratton, Sneden, & Carretta (2004).

Because red giants are bright, mapping the globular cluster abundance patterns has focused historically on giants. In addition, red giants have convective envelopes that mix material to their surfaces that has undergone some H-burning; specifically, anti-correlations between C and N are predicted by theory and observed spectroscopically (e.g. Sweigert & Mengel 1979; Charbonnel et al. 1998; Gratton et al. 2000). Variations in O, Na, Mg, or Al in low-mass giants requires much deeper mixing, and such deep mixing is not predicted by models of low-mass stars. Nonetheless, extra-mixing scenarios can be developed for low-mass red giants and these processes can be invoked to explain the observed anomalous globular cluster abundance patterns (e.g. Langer & Hoffman 1995).

Invoking extra-mixing does not explain why such processes occur in low-mass globular cluster giants, yet are absent in field giants with similar masses, metallicities, and luminosities. In addition, nagging observations of anti-correlated C and N abundances in turn-off and main-sequence globular cluster stars from low-resolution spectra (e.g. Suntzeff & Smith 1991), as well as N and Na correlations in some turn-off stars (Briley et al. 1996) are not

explained by in-situ red giant deep mixing. More recently, a number of high-resolution spectroscopic studies have uncovered the same abundance variations in globular cluster stars near the main sequence as those observed in the same cluster red-giant stars (e.g., Gratton et al. 2001; Ramirez et al. 2001; Ramirez & Cohen 2003). The set of abundance variations among CNO and Na-Mg-Al now observed in globular cluster turn-off stars effectively rules out the presently observed generation of low-mass red giants as the culprits responsible for the anomalous cluster abundances. One must look to another site to produce the hot H-burning abundance patterns specific to the globular clusters.

Another astrophysical site that includes H-burning, mixing, and mass loss which could possibly contaminate an early globular cluster environment is provided by massive asymptotic giant branch (AGB) stars. In massive AGB stars with deep convective envelopes, the envelope bases undergo hot H-burning (hot bottom burning, or HBB); such burning can produce the required CNO and Na-Mg-Al patterns seen in globular clusters. Another signature of HBB would be the destruction of fluorine via  $^{19}\text{F}(p,\alpha)^{16}\text{O}$ . Although  $^{19}\text{F}$  is produced in lower-mass AGB stars (Jorissen et al. 1992), this production becomes efficient destruction in HBB above masses of about  $3.5M_{\odot}$ .

If a generation of massive AGB stars polluted a young cluster environment (where star formation was still ongoing) with slow winds from HBB envelopes, the O, Na, Mg, and Al patterns might be explained. Such a scenario would predict significant  $^{19}\text{F}$  depletions. A clean test of this picture can be carried out using high-resolution IR spectroscopy of HF lines near  $2.2\mu\text{m}$ : such a test in M4 is the goal of this study. The globular cluster M4 was selected, as it is nearby (being perhaps the closest globular cluster) so its members are relatively bright, and its abundance pattern (including N, O, Na, Mg, and Al) was studied extensively by Ivans et al. (1999).

## 2. Observations

The target giants in M4 were a subset of those from Ivans et al. (1999), who analyzed a total of 34 members. A sample of 7 red giants was selected to span the observed range in oxygen and sodium abundances as found by Ivans et al. (1999). We also selected the cooler stars, as these would have stronger HF lines.

High-resolution infrared spectra were obtained with the Gemini South Telescope plus the Phoenix spectrograph (Hinkle et al. 2002) during queue observing in May 2004. The data are single order echelle spectra with a resolution  $R=\lambda/\Delta\lambda=50,000$ , corresponding to a resolution element of  $\sim 4$ -pixels. The observed wavelength is within the K-band, near  $\sim$

23,400Å, containing the molecular HF(1–0) R9 line and numerous CO lines from the 2–0 and 3–1 vibration bands.

The M4 giants are bright in the near-infrared so that total exposure times of 20 minutes were needed to obtain signal-to-noise ratios in excess of  $\sim 300$ . The target stars were observed in different positions on the slit. In addition, hot stars were also observed. These hot star spectra were needed in order to remove telluric lines from the stellar spectra. All the spectra were reduced to one-dimension using standard IRAF routines. More details on the observations and reduction procedures adopted are found in Smith et al. (2002).

A sample Phoenix spectrum is shown in Figure 1 for one of the M4 red giants. Some of the prominent absorption lines are identified, with numerous  $^{12}\text{C}^{16}\text{O}$  lines, along with the HF 1-0 R9 line, as well as a couple of atomic lines from Fe I and Na I.

### 3. Stellar Parameters & Analysis

The Ivans et al. (1999) study was based upon optical high-resolution spectra. The critical parameters needed for an abundance analysis are effective temperature ( $T_{\text{eff}}$ ), surface gravity (parameterized as  $\log g$ ), microturbulent velocity ( $\xi$ ), and overall model atmosphere metallicity. Ivans et al. based their  $T_{\text{eff}}$ -scale on line-depth ratios, as described by Gray (1994). Surface gravities were fixed by enforcing ionization equilibrium for Fe I/Fe II and Ti I/Ti II. These gravities are in generally good agreement with those predicted from model color-magnitude diagrams. Finally, microturbulent velocities were set from the Fe I lines which spanned a large range in equivalent width. The stellar parameters are listed in Table 1, along with the Fe I and Fe II abundances: all taken from Ivans et al. (1999). The stellar designations are from Lee (1977).

The same model atmospheres as used by Ivans et al. (1999) were employed here, which are taken from the MARCS grid (Gustafsson et al. 1975); these models have been found to be quite adequate for stars having the effective temperatures and gravities spanned by the sample here.

The new data added to M4 are the high-resolution IR spectra containing the HF 1–0 R9 line, plus a well-defined sample of  $^{12}\text{C}^{16}\text{O}$  lines (Figure 1). Equivalent widths were measured for 6 CO lines and these values are shown in Table 2. The designations, excitation potentials ( $\chi$ ) and gf-values are taken from Goorvitch & Chackerian (1994 a,b). With the oxygen abundances from Ivans et al. (1999), these CO lines were used to determine  $^{12}\text{C}$  abundances in these stars.

Fluorine abundances were determined from the HF (1-0) R9 line using spectrum synthesis. The line list adopted is described in Smith et al. (2002) and Cunha et al. (2003). Samples of observed and synthetic spectra for two of our targets are shown in Figure 2. Due to the high signal-to-noise of the spectra, the  $^{19}\text{F}$  abundance is well determined. The dependance of the derived fluorine abundances on the stellar parameters was computed and is summarized as follows:  $\delta T_{eff}$  of +100K leads to a increase of +0.22 dex in the fluorine abundance,  $\delta \log g = +0.3$  produces a  $\delta F = -0.11$  dex, and a  $\delta \xi = +0.5 \text{ km s}^{-1}$  results in 0.00 dex change in fluorine. The changes were computed using a baseline model for L1514 of  $T_{eff}=3875 \text{ K}$ ,  $\text{Log } g = 0.35$ , with  $\xi=2.5 \text{ km s}^{-1}$ .

Abundances are summarized in Table 3, with the  $^{12}\text{C}$  and  $^{19}\text{F}$  values derived here, while those of  $^{13}\text{C}$  were re-derived from the M4 data of Ivans et al. (1999), employing our newly derived  $^{12}\text{C}$  values. Also included in the table are O, Na, Mg, and Al taken from Ivans et al. (1999). As the  $^{12}\text{C}$  abundances were derived from 6 lines, the standard deviations are also given in Table 3, which gives some measure of the overall quality of the spectra and the analysis.

The newly derived  $^{12}\text{C}$  abundances here update those of Suntzeff & Smith (1991) and which were employed in Ivans et al. (1999). The  $^{12}\text{C}$  abundances presented by Suntzeff & Smith were derived from low-resolution  $2.2\mu\text{m}$  spectra which were unsuitable for determining microturbulent velocities, thus assumed values of  $\xi$  had to be used. The actual values of  $\xi$  determined from high-resolution optical spectra by Ivans et al. (1999) and from the high-resolution IR spectra here (using the  $^{12}\text{C}^{16}\text{O}$  lines) are considerably lower than those assumed by Suntzeff & Smith (1991); on average for the 7 red giants observed here, the values of microturbulent velocity are  $0.7 \text{ km s}^{-1}$  lower. This increases the  $^{12}\text{C}$  abundances significantly. Even with this increase, the effect of decreasing carbon-12 abundance with increasing red-giant luminosity found by Suntzeff & Smith (1991) is confirmed for the stars observed. We illustrate this in Figure 3, where the  $^{12}\text{C}$  abundance is plotted versus the red-giant bolometric magnitude.

The fluorine abundances show much larger scatter than the abundance uncertainties. Ivans et al. (1999) found large scatter in the other abundances of C, N, O, Na, Mg and Al, as discussed in the introduction. Here we show that fluorine behaves in a similar manner to these other elements. The addition of fluorine to the list of elements found to vary in the globular cluters has implications for the types of progenitor stars that produce these abundance variations.

In addition to fluorine, the newly derived  $^{12}\text{C}$  abundances can be added to those of  $^{13}\text{C}$ ,  $^{14}\text{N}$ , and  $^{16}\text{O}$  to form the total sum of C+N+O and this is shown in Table 3. This sum is constant to high accuracy for all stars studied with a mean and standard deviation

of  $C+N+O=8.17\pm 0.08$ : the scatter can be accounted for entirely by analysis errors. The constancy of  $C+N+O$  limits strongly the addition of any primary  $^{12}\text{C}$  from  $^4\text{He}$ -burning and third dredge-up on the AGB.

#### 4. Discussion

In the introduction we discussed how globular clusters show specific abundance variations centered on the elements C, N, O, Na, Mg, and Al (with a current summary in Gratton et al. 2004). With the increasing numbers of globular cluster main-sequence stellar abundance studies demonstrating that these abundance variations must arise from early chemical evolution within the globular clusters, we will use the M4 chemical inhomogeneities (including fluorine) to define quantitative chemical yields required from these progenitor stars.

Figure 4 summarizes the abundance variations observed in M4. We choose to use Na as a comparison element and then plot  $[X/\text{Fe}]$  vs  $[\text{Na}/\text{Fe}]$  for the elements O, F, Mg, Al, Ti and La. We do not include C and N in this plot, because low-mass red-giant mixing alters these abundances anyway, thus obscuring any primordial signatures. The filled symbols in Figure 4 are the stars observed here for HF, while the open symbols are all other stars from Ivans et al. (1999); approximate error bars are plotted for stars observed for this study. As known previously, oxygen decreases as Na increases, while Al increases with Na. We show here for the first time that fluorine decreases as Na increases, with an even larger variation than oxygen. As expected, Ti does not vary with Na. La does not vary either, which precludes any significant contribution from the s-process. Except for one star from the Ivans’ sample, Mg does not seem to change significantly with Na.

Adding fluorine to the suite of elements whose abundances vary in M4 provides another constraint on the underlying nucleosynthesis pattern. We proceed to define this pattern based on the simple model for chemical enrichment in M4. The assumption is that the oxygen-high, sodium-low stars define the initial chemical mix in M4. Some mass range within this stellar generation added ejecta to the M4 intracluster environment which bore the signature of hydrogen burning in the CNO, Ne-Na, Mg-Al cycles. This material did not originate in massive stars as there is no evidence of significant variations in elements that arise from SN II (such ejecta could have escaped from the intra-cluster medium due to high velocity). In order to understand the chemical history in M4, it is crucial to pin down the mass range of the polluting stars. In this model a new generation (or generations) of stars formed from differing fractions of this stellar ejecta thus producing the observed abundance inhomogeneities. We used the distributions in Figures 4 to define the initial abundances of oxygen, fluorine, sodium, magnesium, and aluminium. Final abundances,

which would represent the extreme case of pure ejecta, are defined by the most Na-rich part of the distributions. These initial and final abundances are tabulated in Table 4, as well as the final - initial abundances expressed as a mass fraction.

The mass fractions shown in Table 4 represent the yields that were produced by the polluting stars. These yields are qualitatively what is expected from H-burning at temperatures of about 50 MK. What is of special importance is the rather large depletion of fluorine. Based on models by Fenner et al. (2004) stars with masses less than about 3.5 solar masses are net producers of fluorine during AGB evolution. Our results rule out stars of this mass or less as being significant contributors to chemical evolution within M4. These observationally derived yields can be used to constrain even more tightly the mass range of the polluting stars. As a simple illustration, we show in Figure 5 predicted mass yields from HBB AGB model stars as a function of stellar mass for masses of 3.5, 5.0, and 6.5 solar masses for the elements of interest here. Superimposed on this we also show the estimated yields from Table 4. The importance of fluorine can be seen from this comparison as its yield is a steep function of stellar mass and covers both positive and negative values. This is a simple, but promising comparison illustrating reasonable qualitative agreement, but quantitative agreement remains lacking. At the observed level of the fluorine and oxygen depletions, the Na, Mg and Al enhancements predicted by the models appear to be too large. Of course, the yields shown in Figure 5 need to be convolved with an IMF; however, a simple convolution shows that the lower mass stars tend to dominate.

The estimation of the observed abundance yields plotted in Figure 5 are based upon a very simple chemical evolutionary model for M4. Better agreement between the stellar models and the observed estimated chemical yields might be achieved with additions to the simple model. For example, it might be that some of the original stars had even lower Na and Al abundances than those estimated here. Another possibility is that AGB stars even more massive than  $6.5M_{\odot}$  may provide a better comparison. There might also be less dilution of CNO-processed material in the real stars when compared to the models. Observations of more globular clusters, especially those having different metallicities, will be useful in future comparisons of observed abundance trends with stellar model predictions.

## 5. Conclusions

We present the first fluorine abundances derived in a globular cluster that show variations which correlate with the oxygen abundances and anti-correlate with the Na and Al variations. Because the predicted fluorine yields are a strong function of stellar mass, fluorine abundances can be used as a significant constraint in defining the nature of the progenitor

stars responsible for driving chemical evolution in globular clusters. Knowledge of the mass range of these stars would provide strong limits on the timescales for early star formation in a proto-globular cluster environment. Our results are in qualitative agreement with HBB AGB models, but strict quantitative agreement remains elusive; however, the combination of more abundances in other clusters, particularly fluorine, coupled with further efforts in stellar modelling may yield the desired agreement.

## 6. Acknowledgements

Based on observations obtained at the Gemini Observatory, which is operated by the Association of Universities for Research in Astronomy, Inc., under a cooperative agreement with the NSF on behalf of the Gemini partnership: the National Science Foundation (United States), the Particle Physics and Astronomy Research Council (United Kingdom), the National Research Council (Canada), CONICYT (Chile), the Australian Research Council (Australia), CNPq (Brazil), and CONICRT (Argentina), as program GS-2004A-Q-20. This paper uses data obtained with the Phoenix infrared spectrograph, developed and operated by the National Optical Astronomy Observatory. This work is also supported in part by the National Science Foundation through AST03-07534 (VVS), NASA through NAG5-9213 (VVS), and AURA, Inc. through GF-1006-00 (KC). I.I. is pleased to acknowledge research support from NASA through Hubble Fellowship grant HST-HF-01151.01-A from the Space Telescope Science Inst., operated by AURA, under NASA contract NAS5-26555. We wish to thank the anonymous referee for useful comments that improved this paper.



## REFERENCES

- Briley, M. M., Smith, V.V., Suntzeff, N. B. & Lambert, D. L. 1996, *Nature*, 383, 604
- Charbonnel, C., Brown, J.A., & Wallerstein, G. 1998, *A & A*, 332, 204
- Cunha, K., Smith, V.V., Lambert, D.L. & Hinkle, K.H., 2003, *ApJ*, 126, 1305
- Fenner, Y., Campbell, S., Karakas, A.I., Lattanzio, J.C., Gibson, B.K., 2004, *MNRAS*, 353, 789
- Goorvitch, D., Chackerian, C., Jr. 1994, *ApJS*, 91, 483
- Goorvitch, D., Chackerian, C., Jr. 1994, *ApJS*, 92, 311
- Gray, D. F. 1994, *PASP*, 106, 1248
- Gratton, R., Sneden, C. & Carretta, E. 2004, *ARAA*, 42, 385
- Gratton, R., and 16 co-authors 2001, *A&A*, 369, 87
- Gratton, R., Sneden, C., Carretta, E., & Bragaglia, A. 2000, *A&A*, 354, 169
- Gustafsson, B., Bell, R. A., Eriksson, & K., Nordlund, A. 1975, 42, 407
- Hinkle, K. H., Blum, R., Joyce, R. R., Ridgway, S. T., Rodgers, B., Sharp, N., Smith, V., Valenti, J., & van der Bliik, N. 2002, *SPIE*, 4834, 353
- Ivans, I. I., Sneden, C., Kraft, R. P., Suntzeff, N. B., Smith, V. V., Langer, G. E., Fulbright, J. P. 1999, 118, 1273
- Jorissen, A., Smith, V.V., & Lambert, D.L. 1992, *A&A*, 261, 164
- Langer, G. E., & Hoffman, R. D. 1995, *PASP*, 107, 1177
- Lee, S. W. 1977, *A&AS*, 27, 367
- Ramirez, S.V., Cohen, J.G., Buss, J., & Briley, M.M. 2001, *AJ*, 122, 1429
- Ramirez, S.V., & Cohen, J.G. 2003, *AJ*, 125, 224
- Smith, V.V., Hinkle, K.H., Cunha, K., Plez, B., Lambert, D.L., Pilachowski, C.A., Barbuy, B., Melendez, J., Balachandran, S., Bessel, M.S., Geisler, D.P., Hesser, J.E., & Winge, C. 2002, *AJ*, 124, 3241
- Suntzeff, N. B., & Smith, V. V. 1991, *ApJ*, 381, 160

Sweigart, A. V., & Mengel, J. W. 1979, ApJ, 229, 624

Table 1. Stellar Parameters

Star	$T_{\text{eff}}(\text{K})$	$\text{Log } g \text{ (cm s}^{-2}\text{)}$	$\xi \text{ (km s}^{-1}\text{)}$	$A(\text{Fe I})^a$	$A(\text{Fe II})^a$
1411	3950	+0.60	1.65	6.29	6.32
1514	3875	+0.35	1.95	6.27	6.42
2307	4075	+0.85	1.45	6.30	6.33
3209	3975	+0.60	1.75	6.28	6.32
3413	4175	+1.20	1.65	6.32	6.35
4611	3725	+0.30	1.70	6.34	6.33
4613	3750	+0.20	1.65	6.31	6.35

Note. — (a):  $A(\text{X}) = \log[n(\text{X})/n(\text{H})] + 12$ . The solar iron abundance is  $A(\text{Fe})_{\odot} = 7.45$ .

Table 2.  $^{12}\text{C}^{16}\text{O}$  Lines and Equivalent Widths

$\lambda(\text{\AA})$	$\chi(\text{eV})$	Log gf	Line ID	1411 <sup>a</sup>	1514 <sup>a</sup>	2307 <sup>a</sup>	3209 <sup>a</sup>	3413 <sup>a</sup>	4611 <sup>a</sup>	4613 <sup>a</sup>
23302.949	1.421	-4.517	3-1 R70	159	248	160	221	176	238	250
23303.959	0.485	-4.996	3-1 R30	392	476	368	468	408	456	482
23340.590	0.431	-5.064	3-1 R26	382	515	360	460	388	474	498
23367.117	0.005	-6.338	2-0 R4	241	388	208	314	247	336	346
23372.385	0.396	-5.124	3-1 R23	350	484	336	434	348	457	474
23373.398	1.657	-4.456	3-1 R77	130	233	126	196	152	183	168

Note. — (a): Equivalent width in mÅ.

Table 3. Abundances<sup>a</sup>

Star	A( <sup>12</sup> C)	A( <sup>19</sup> F)	<sup>12</sup> C/ <sup>13</sup> C	A( <sup>14</sup> N)	A(O)	A(Na)	A(Mg)	A(Al)	A(C+N+O)
1411	7.08 ±0.08	2.90	4.0	7.70	7.93	5.45	6.66	6.01	8.177
1514	7.28 ±0.11	3.15	5.0	7.18	8.18	5.07	6.77	5.70	8.277
2307	7.24 ±0.07	3.10	5.0	7.47	7.91	5.42	6.78	5.97	8.119
3209	7.34 ±0.07	3.20	5.0	7.20	8.00	5.25	6.85	5.93	8.153
3413	7.45 ±0.10	3.35	4.0	6.96	8.16	5.01	6.74	5.87	8.276
4611	7.17 ±0.04	2.70	5.0	7.72	7.81	5.39	6.70	5.86	8.130
4613	7.09 ±0.05	2.88	4.0	7.55	7.81	5.31	6.72	5.88	8.062
Sun	8.39	4.55	89	7.78	8.66	6.17	7.53	6.37	8.884

Note. — (a):  $A(X) = \log[n(X)/n(H)] + 12$ . The <sup>12</sup>C, <sup>13</sup>C and <sup>19</sup>F abundances are from this study, while the other abundances are from Ivans et al. (1999).

Table 4. Observationally Derived Chemical Yields for M4

Element	$A(x)_{init}$	$A(x)_{fin}$	$\text{Log} (A(x)_{fin} - A(x)_{init})$
O	7.98	7.62	-0.36
F	3.35	2.68	-0.67
Na	4.82	5.49	+0.67
Mg	6.74	6.76	+0.02
Al	5.66	5.95	+0.29
Ti	4.00	4.01	+0.01
La	0.38	0.38	0.00

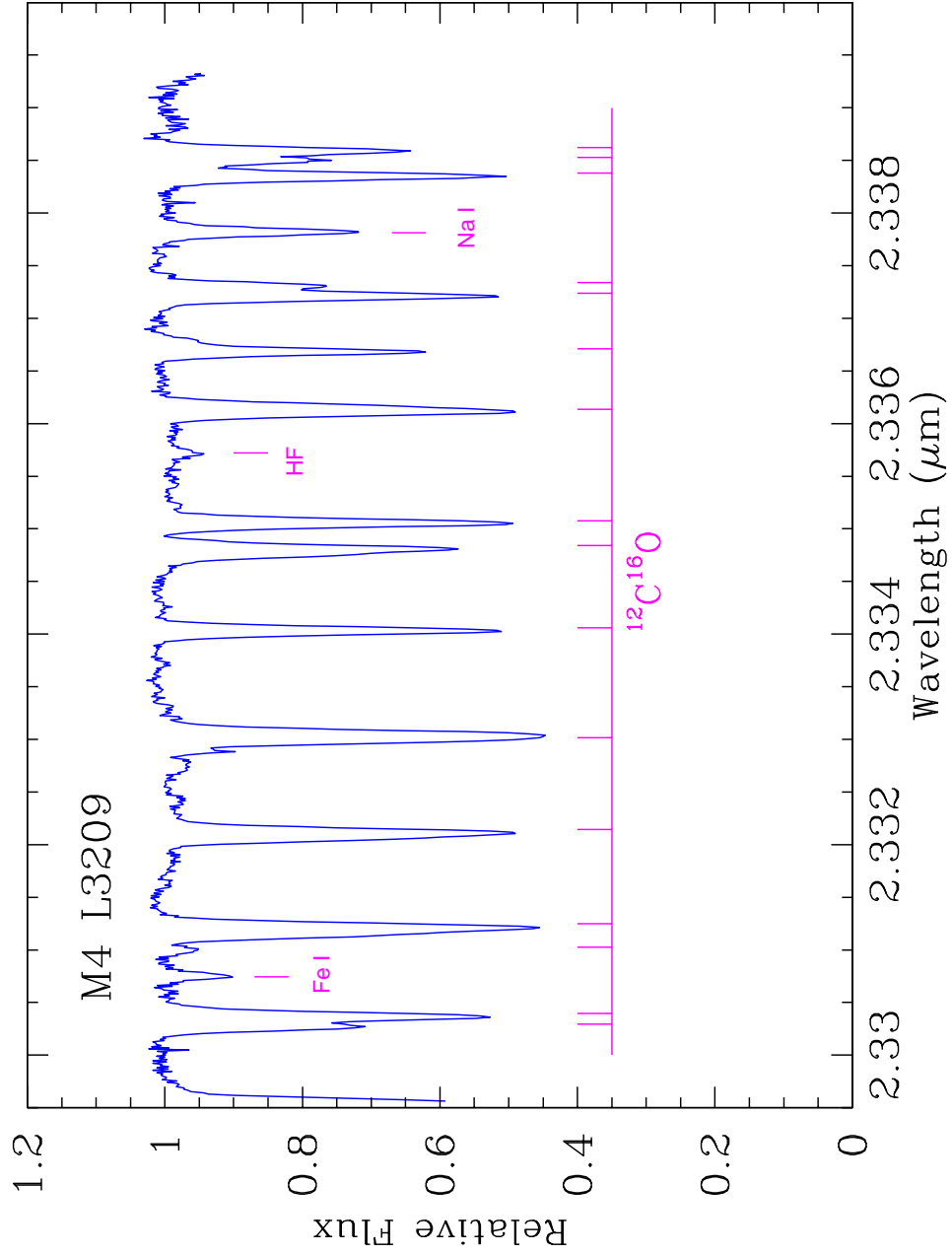


Fig. 1.— Observed Phoenix spectra for the M4 red giant Lee 1411 centered at 23390 Å. Prominent absorption lines are labelled.

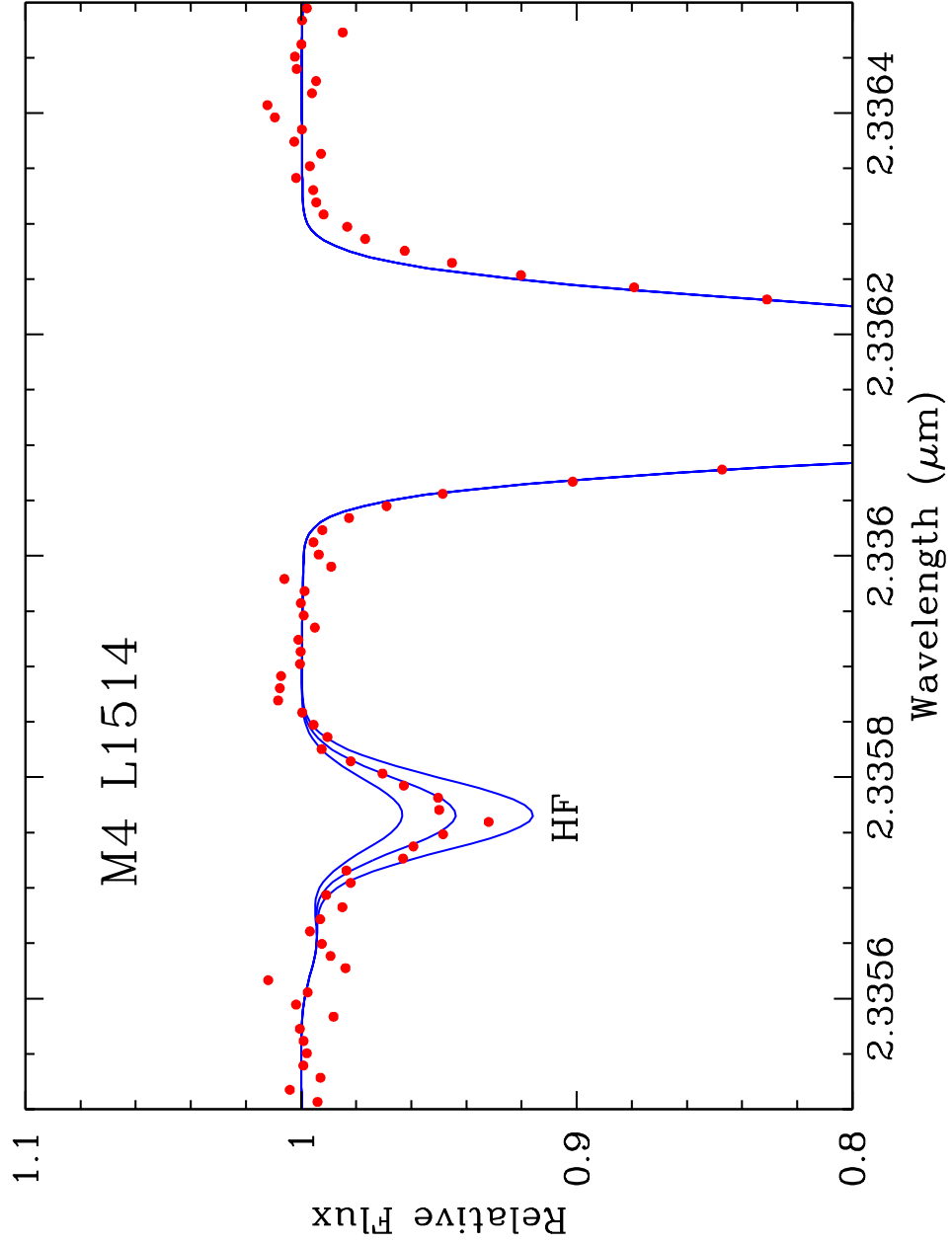


Fig. 2.— Observed and synthetic spectra for target star M4 Lee1514 in the HF region. The best-fit fluorine abundances (represented by the middle solid line) is that presented in Table 3. The synthetic spectra were calculated with  $\pm 0.2$  dex changes in the  $^{19}\text{F}$  abundance.



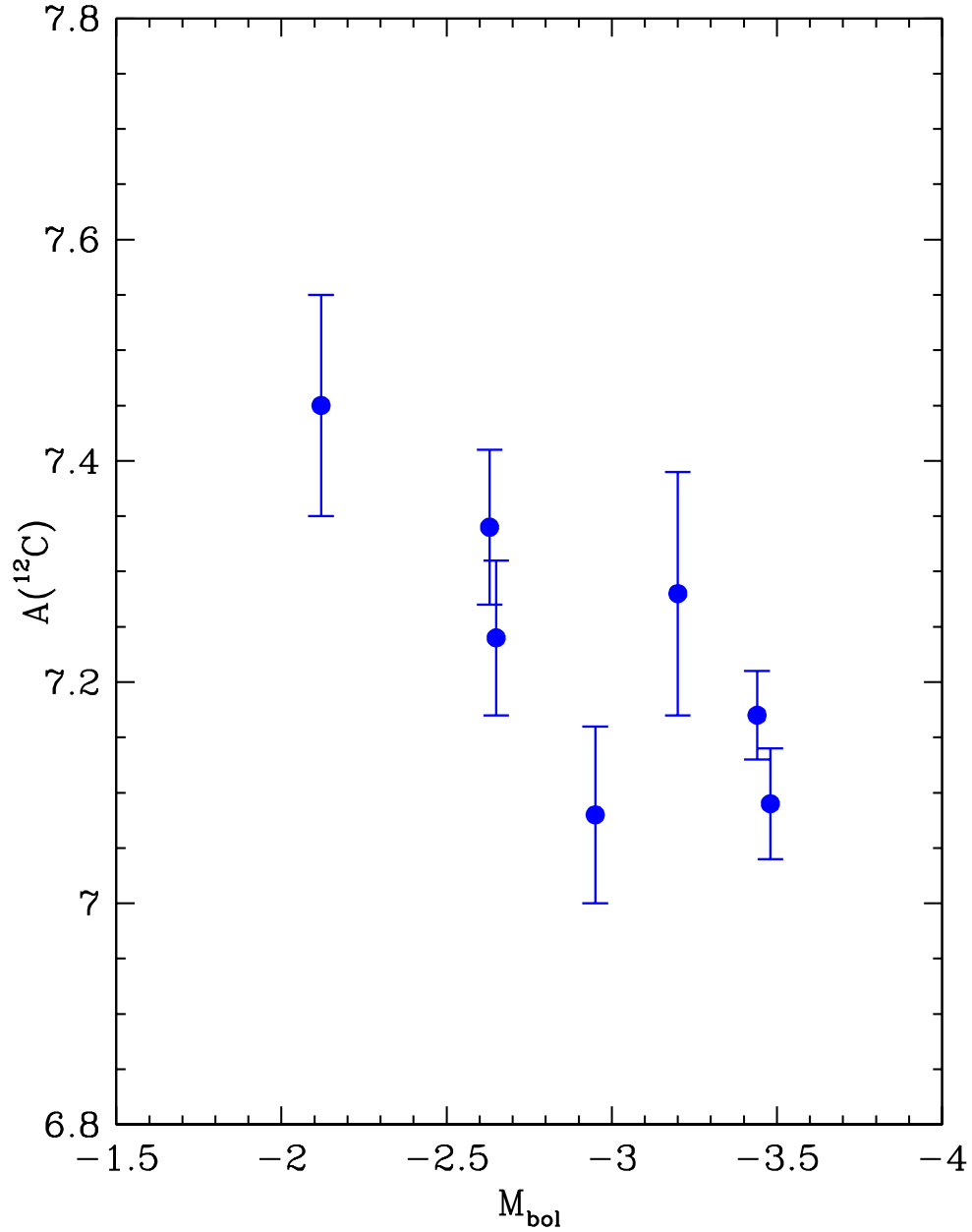


Fig. 3.— Carbon-12 abundances versus  $M_{bol}$  for the seven M4 red giants observed here ( $M_{bol}$  values are taken from Ivans et al. 1999). The decreasing  $^{12}C$  abundance with increasing red-giant luminosity noted for M4 by Suntzeff & Smith (1991) is also found using updated  $^{12}C$  abundances.

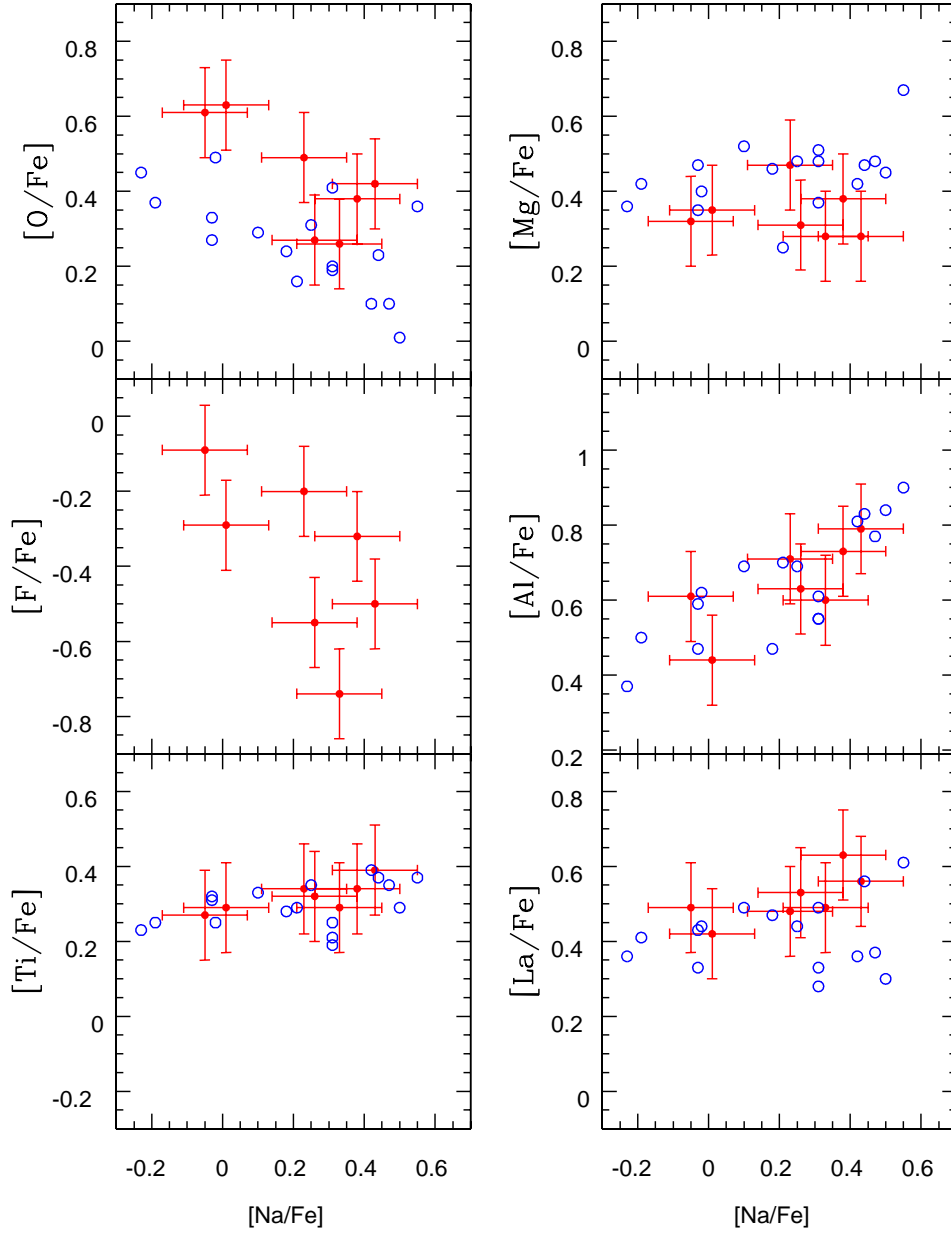


Fig. 4.— Six elemental abundance ratios (measured relative to Fe) plotted versus  $[\text{Na}/\text{Fe}]$  for stars in M4. The solid circles are target stars observed for HF and the open circles are all other stars from Ivans et al. (1999). Note the significant anti-correlation of  $[\text{F}/\text{Fe}]$  with  $[\text{Na}/\text{Fe}]$ , as was found previously for  $[\text{O}/\text{Fe}]$  versus  $[\text{Na}/\text{Fe}]$ , while  $[\text{Al}/\text{Fe}]$  increases with  $[\text{Na}/\text{Fe}]$ . No significant trends (of about 0.05 to 0.10 dex per dex) are observed for  $[\text{Mg}/\text{Fe}]$ ,  $[\text{Ti}/\text{Fe}]$ , or  $[\text{La}/\text{Fe}]$  with  $[\text{Na}/\text{Fe}]$ .

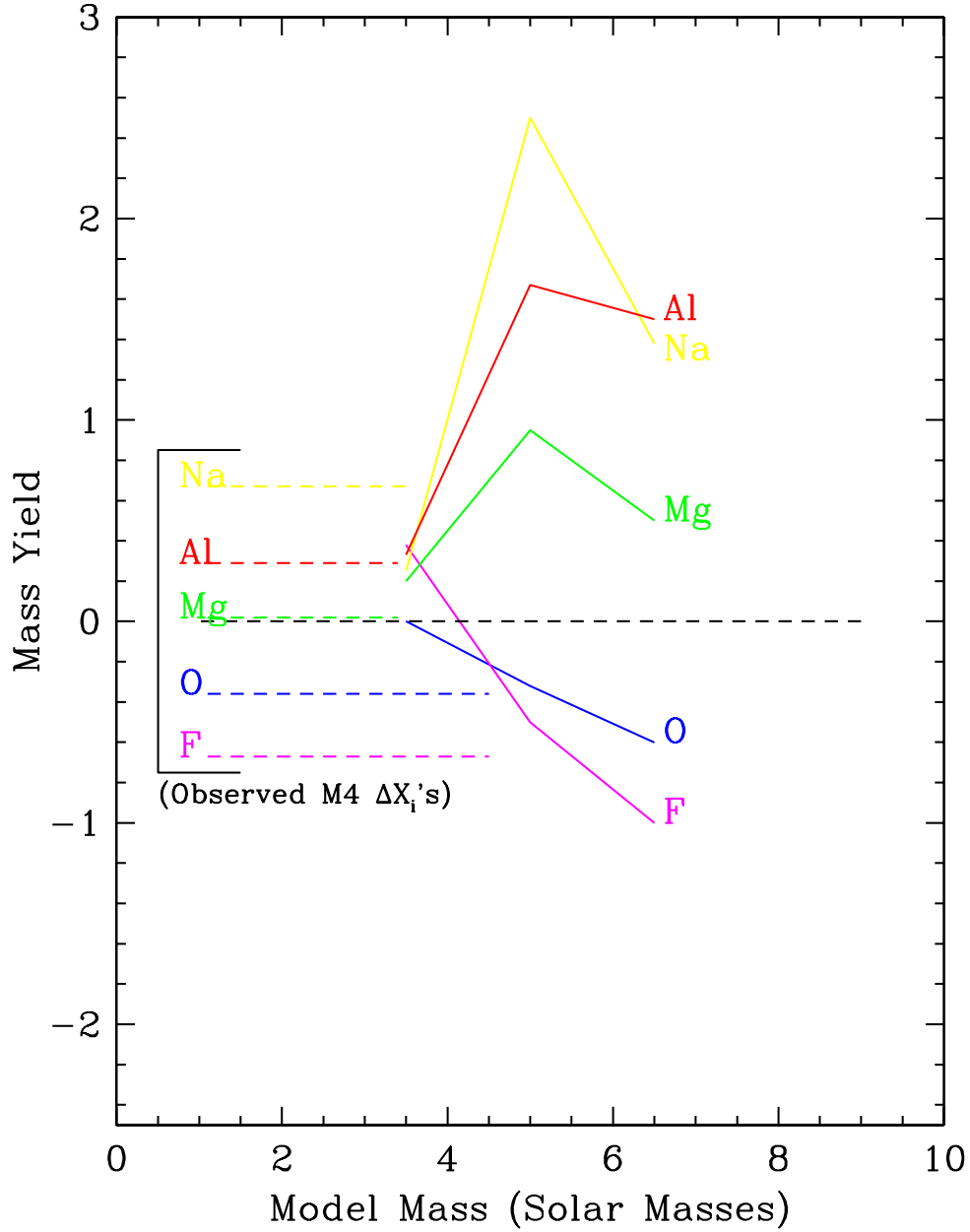


Fig. 5.— Predicted mass yields from stellar models undergoing HBB on the AGB (solid lines); these are taken from Fenner et al. (2004) which were used in an analysis of NGC6752 abundances. The dashed lines are the observationally derived mass yields for M4 from this study. Detailed agreement between observations and models is still lacking, however, there is rough agreement for the bulk abundances of O, F, Na, Mg and Al.